**Computers and Concrete**, *Vol. 24, No. 6 (2019) 513-525*
DOI: https://doi.org/10.12989/cac.2019.24.6.513


# Damage and stiffness research on steel shape steel fiber reinforced concrete composite beams

Chao Xu[1,2a], Kai Wu*[1], Ping zhou Cao[1], Shi qi Lin[1] and Teng fei Xu[2]

[1]*College of Civil and Transportation Engineering, Hohai University, Nanjing 210098, China*
[2]*Institute of Civil and Architectural Engineering, Tongling University, Tongling 244000, China*

(*Received August 28, 2019, Revised October 14, 2019, Accepted October 13, 2019*)

**Abstract.** In this work, an experimental research has been performed on Steel Fiber-Steel Reinforced Concrete (SFSRC)specimens subjected to four-point bending tests to evaluate the feasibility of mutual replacement of steel fibers and conventional reinforcement through studying failure modes, load-deflection curves, stiffness of characteristic points, stiffness degradation curves and damage analysis. The variables considered in this experiment included steel fiber volume percentage with and without conventional reinforcements (stirrups or steel fibers) with shear span depth ratios of S/D=2.5 and 3.5. Experimental results revealed that increasing the volume percentage of steel fiber decreased the creation and propagation of shear and bond cracks, just like shortening the stirrups spacing. Higher crack resistance and suturing ability of steel fiber can improve the stability of its bearing capacity. Both steel fibers and stirrups improved the stiffness and damage resistance of specimens where stirrups played an essential role and therefore, the influence of steel fibers was greatly weakened. Increasing S/D ratio also weakened the effect of steel fibers. An equation was derived to calculate the bending stiffness of SFSRC specimens, which was used to determine mid span deflection; the accuracy of the proposed equation was proved by comparing predicted and experimental results.

**Keywords:** steel-reinforced concrete composite structure; steel fiber-reinforced concrete; stiffness; damage resistance; bending stiffness equation

## 1. Introduction

Steel-reinforced concrete (SRC) structures are widely used in large span and high-rise buildings due to their excellent properties such as great stiffness, high bearing capacity, small section size and outstanding ductility performance (Wu *et al.* 2018). However, the complexity of the construction process, difficulties in the binding of steel reinforcement during the whole construction stage that prolongs the construction period and increases the difficulty of construction. As shown in Fig. 1, steel bars always need to perforate the flanges and web of steel shape to maintain continuous reinforcement which increases the difficulty of steel shape processing and steel bar binding and decreases the bending and shear resistance of steel shape (Foraboschi 2016). Replacing steel bars with steel fibers is an economically and efficiently beneficial solution to address this problem. Many researchers have demonstrated that the addition of steel fibers into concrete not only remarkably improves the toughness and post-cracking energy absorption characteristics of the concrete (Fantilli *et al.* 2011, Jang and Yun 2018), but also significantly enhances its compressive (Eltobgy 2013), flexural (Won *et al.* 2012) and tensile (Xu *et al.* 2017) strength. Moreover, steel fibers are considered as an alternative for traditional reinforced concrete specimens with improved shear and flexural bearing capacity and ductility (Aoude *et al.* 2012, Biolzi and Cattaneo 2017, Biolzi *et al.* 2000, Ding *et al.* 2012, Dinh *et al.* 2010, Kim *et al.* 2012, Xu *et al.* 2016, Xu *et al.* 2017). The fib Model Code for Concrete Structures 2010

(a) Beam-column joints

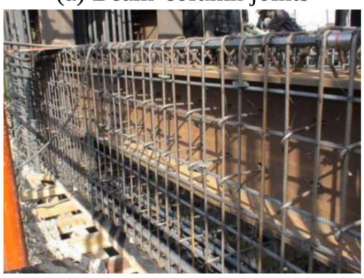

(b) Normal SRC beam

Fig. 1 Construction difficulties of steel reinforced concrete

*Corresponding author, Associate Professor
E-mail: Wukai19811240@163.com
[a]Ph.D.
E-mail: chaoxu0613@163.com


http://www.techno-press.org/?journal=cac&subpage=8
ISSN: 1598-8198 (Print), 1598-818X (Online)

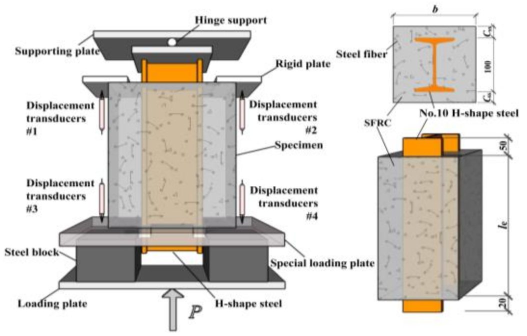


(a) Test arrangement

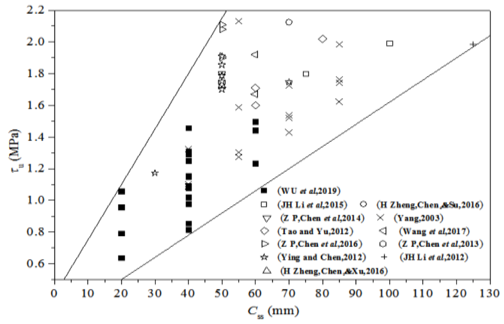

(b) The comparison between the tested results and collected data

Fig. 2 Nominal bond strength of SRC (Wu *et al.* 2019)

(MC2010) (FIB 2013) and ACI 318 (ACI318-11 2011) have already stated that conventional stirrups can be replaced with steel fibers, which has been recognized as a proper construction material. More importantly, ACI 318-11 Code has stated that partial replacement of minimum shear reinforcement with fiber amounts of greater than 0.75% of the total concrete volume (crimped or hooked fibers) could be used for concretes with strengths of lower than 40 MPa and beam depths of lower than 60 cm. However, many experimental research works and national specifications concerning SRC composite structures have found bond-slip behaviors between shaped steel and surrounding concrete which have great influence on the load-bearing capacities of SRC structures (JGJ138-2016 2016, YB9082-2006 2006, European Code 4 2014, Zheng *et al.* 2003). If steel fibers are used to replace a part or all of the conventional reinforcements, the combined action between steel shape and steel fiber concrete should be ensured.

We conducted 16 bond slip tests on different steel fiber-steel reinforced concrete specimens without conventional reinforcement, including 8 circular and 8 square section specimens (Wu *et al.* 2019). Fig. 2 presents research data on the bonding properties of steel-reinforced concrete specimens obtained by different researchers (their specimens highly correlated with ours) and statistically compares them with our findings. According to statistical results, interfacial bonding strength between steel shape and steel fiber concretes was slightly lower than that of normal steel-reinforced concrete specimens with the same protective concrete layer thickness. This experiment laid a foundation for testing the bending performance of steel fiber-reinforced concrete composite beams. Therefore, it could be expected that the addition of steel fibers into conventional SRC beams would not only increase their load bearing capacity and ductility but also improve their bending stiffness and damage development. The feasibility of replacing conventional reinforcements with steel fibers in SRC structures needs further evaluation.

To the best of our knowledge, limited research has been performed on the calculation of the bending stiffness of fiber-reinforced concrete structural elements with conventional reinforcement. However, the most practical suggestion can be found in the Chinese code CECS 38:2004 (38-2004 2004) where stiffness influence coefficient is introduced to reflect the crack resistance of steel fibers based on stiffness calculation method in ordinary reinforced concrete beams. Research in this field is still insufficient and the obtained results show disagreement. Gao and Zhang (2013) proved that the bending stiffness calculated according to CECS 38:2004 was clearly overestimated compared with experimental values. Calculation of bending stiffness in SRC beams with conventional reinforcements has been the subject of many publications. Calculation methods can be roughly divided into three categories: deformation compatibility, stiffness superposition and stiffness reduction. The most practical method is stiffness superposition method due to its high practical operability which is also recommended in European Code 4 and JGJ138-2016 pre-standard. SRC bending stiffness is the superposition of the bending stiffnesses of steel shape, steel bar and concrete according to European Code 4; correction factor was considered when calculating concrete stiffness. The Chinese codes JGJ138-2016 and YB9082-2006 have assumed SRC bending stiffness as the superposition of bending stiffnesses of steel shape and reinforced concrete (JGJ138-2016 2016, YB9082-2006).

In this paper, failure modes, bearing capacities, load-deflection curves, stiffness and damage were investigated to determine the combined effect of steel bar and steel fibers on the behavior of SFSRC specimen. Four point bending tests were performed on 18 tested SFSRC specimens. The variables considered in tests were shear span-effective depth ratio (2.5 and 3.5), presence and absence of longitudinal reinforcement, stirrup spacing (180 mm, 360 mm and ∞) and steel fiber volume percentage (0, 1 and 2%). Moreover, prediction equations were proposed to calculate the bending stiffness of SFSRC beams based on CECS 38:2004 and JGJ138-2016 methods. Midpoint deflection was be calculated by bending stiffness equation using structural mechanics method.

## 2. Test program

### 2.1 Test specimen

SFRC mix used in this experiment was produced based on Chinese Steel Fiber Reinforced Concrete codes JG/T 472-2015 (472-2015, 2015) and JGJ55-2011 (55, 2011). River sand with the density of 2650 kg/m$^3$ was obtained from a local sand factory and was used as fine aggregate. Conch cement P.O 42.5 (3100 kg/m$^3$) was applied as binder. Other ingredients were: crushed stone (2800 kg/m$^3$), normal water and shear rippled steel fibers with aspect ratio

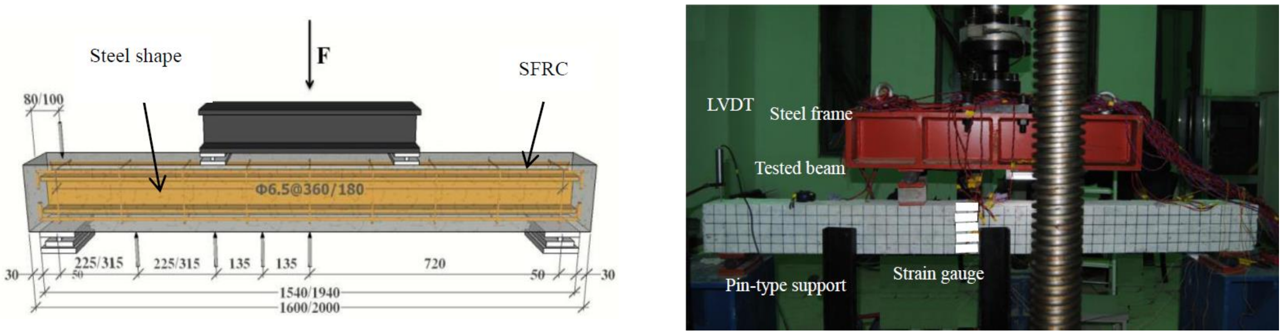


(a)Test arrangement

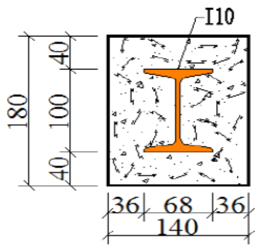


(b)Beams without steel rebar

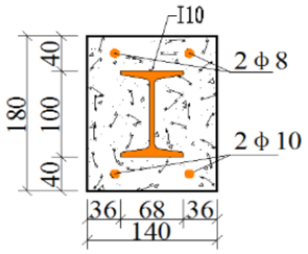


(c)Beams with longitudinal bar

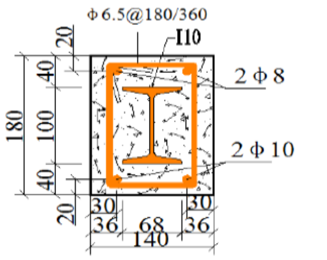


(d)Beams with conventional reinforcement

Fig. 3 Test arrangement and three types of cross section (unit: mm)

$\lambda=l/d=50$ ($l$=30 mm, $d$=0.6 mm). The ultimate tensile strength of steel fiber as higher than 692 MPa. Steel fiber volume contents of 0, 1 and 2% were applied in experiments. The calculated water cement ratio $W/B$ was equal to 0.48 and designed sand rate was 0.38. In order to prepare SFRC mix, dry ingredients including crushed stone, cement and river sand were added into concrete mixer one by one and mixed (2 min) and then, water was added (mixing time 5 min). Steel fibers were added into the mixture at a rate of 15 kg/min, as the final ingredient. Then, mixing was continued at high speed for 5 min. The quantities of all ingredients used for the preparation of specimens are shown in Table 2.

18 composite beams were cast and divided into three types. The first type included 6 SFSRC specimens with different steel fiber percentages in the range of 0% to 2% to evaluate the effect of steel fibers on the failure mode, damage and stiffness of SFSRC beams without conventional reinforcements. In stage 2, the influence of steel fibers in beams with longitudinal reinforcement was evaluated based on the same procedure. In this stage, longitudinal bars were added into specimens of stage 1. Also, it was evaluated whether stirrups were fully replaced with steel fibers. The second stage included 4 specimens with longitudinal reinforcements and steel fibers. 8 beams with steel fibers and conventional reinforcements were tested in stage 3 to investigate the enhancement effect of steel fibers on normal SRC beams. Also, the combined effect and partial substitution between different steel fibers contents (1% and 2%) and stirrups (diameter $\varphi$ 6.5/180, 360 mm) were evaluated. Mechanical properties of the conventional reinforcements used in this experiment are summarized in Table 3. I10 of Q235 grade steel shape was used in all beams; the detailed properties of steel shape are listed in Table 1 and the yield ($f_{wy}$) and ultimate ($f_{wu}$) strength of steel web, the yield ($f_{fy}$) and ultimate ($f_{fu}$)

Table 1 Material properties of steel shape

| Properties | Steel shape I10 | Section size |
|---|---|---|
| $f_{wy}$ | 281.87 MPa | 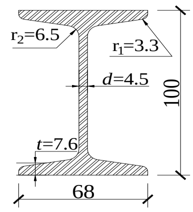 |
| $f_{wu}$ | 409.09 MPa | |
| $E_w$ | 2.03×105 MPa | |
| $f_{fy}$ | 261.71 MPa | |
| $f_{fu}$ | 402.73 MPa | |
| $E_f$ | 1.99×105 MPa | |



strength of steel flange, and elastic modulus of steel web ($E_w$) and flange ($E_f$) are also provided.

As illustrated in Fig. 3, the height and width of all specimens were 180 mm and 140 mm, respectively. The length of beams were divided into 1600 mm and 2000 mm, which meant that $S/D$ ratios were 2.5 and 3.5, respectively. Longitudinal tension reinforcement ratio was kept constant at 0.801%, which was consisted of two steel bars 10 mm in diameter each with a clear concrete cover of 20 mm thickness. Shear reinforcement was consisted of closed stirrups with diameter 6.5 and 180 or 360 mm spacing. For each beam, three series of standard cube concrete specimens (150 mm×150 mm×150 mm) with three different steel fiber volume contents (0%, 1% and 2%) at 28 days were tested as presented in Table 2.

All beams were cast and kept at 20±2°C in moulds. After about 48 hours, beams were demoulded and cured in cement concrete standard curing box for the next 28 days. The beams were loaded 3 days after demoulding since strain gauges on concrete should be installed.

The beams were noted as BA-C-D-E where "$B$" means SFSRC beam, "$A$" means whether to Configure Longitudinal Bars ($X$ for employing longitudinal reinforcement, $Y$ for none), "$C$" is the percentages of steel fiber (in %), "$D$" is the $S/D$ ratio, "$E$" is the stirrup spacing

Table 2 Summary of twenty one SFSRC specimens

| Specimen | Length | $S/D$ | Water (kg/m$^3$) | Cement (kg/m$^3$) | Sand (kg/m$^3$) | Stone (kg/m$^3$) | $\rho_{sf}$ (%) | $f_{cm}$ (MPa) | Stirrups | Longitudinal Reinforcement |
|---|---|---|---|---|---|---|---|---|---|---|
| BY-0-2.5-∞ | 1600 | 2.5 | 185.00 | 385.4 | 719.4 | 1173.8 | 0 | 27.6 | - | - |
| BY-1-2.5-∞ | 1600 | 2.5 | 185.00 | 385.4 | 738.2 | 1125.9 | 1 | 27.5 | - | - |
| BY-2-2.5-∞ | 1600 | 2.5 | 185.00 | 385.4 | 757.0 | 1078.1 | 2 | 28.4 | - | - |
| BX-1-2.5-360 | 1600 | 2.5 | 185.00 | 385.4 | 738.2 | 1125.9 | 1 | 27.5 | $\varphi$6.5@360 | 2$\varphi$8+2$\varphi$10 |
| BX-2-2.5-360 | 1600 | 2.5 | 185.00 | 385.4 | 757.0 | 1078.1 | 2 | 28.4 | $\varphi$6.5@360 | 2$\varphi$8+2$\varphi$10 |
| BX-1-2.5-180 | 1600 | 2.5 | 185.00 | 385.4 | 738.2 | 1125.9 | 1 | 27.5 | $\varphi$6.5@180 | 2$\varphi$8+2$\varphi$10 |
| BX-2-2.5-180 | 1600 | 2.5 | 185.00 | 385.4 | 757.0 | 1078.1 | 2 | 28.4 | $\varphi$6.5@180 | 2$\varphi$8+2$\varphi$10 |
| BX-1-2.5-∞ | 1600 | 2.5 | 185.00 | 385.4 | 738.2 | 1125.9 | 1 | 27.5 | - | 2$\varphi$8+2$\varphi$10 |
| BX-2-2.5-∞ | 1600 | 2.5 | 185.00 | 385.4 | 757.0 | 1078.1 | 2 | 28.4 | - | 2$\varphi$8+2$\varphi$10 |
| BY-0-3.5-∞ | 2000 | 3.5 | 185.00 | 385.4 | 719.4 | 1173.8 | 0 | 27.6 | - | - |
| BY-1-3.5-∞ | 2000 | 3.5 | 185.00 | 385.4 | 738.2 | 1125.9 | 1 | 27.5 | - | - |
| BY-2-3.5-∞ | 2000 | 3.5 | 185.00 | 385.4 | 757.0 | 1078.1 | 2 | 28.4 | - | - |
| BX-1-3.5-360 | 2000 | 3.5 | 185.00 | 385.4 | 738.2 | 1125.9 | 1 | 27.5 | $\varphi$6.5@360 | 2$\varphi$8+2$\varphi$10 |
| BX-2-3.5-360 | 2000 | 3.5 | 185.00 | 385.4 | 757.0 | 1078.1 | 2 | 28.4 | $\varphi$6.5@360 | 2$\varphi$8+2$\varphi$10 |
| BX-1-3.5-180 | 2000 | 3.5 | 185.00 | 385.4 | 738.2 | 1125.9 | 1 | 27.5 | $\varphi$6.5@360 | 2$\varphi$8+2$\varphi$10 |
| BX-2-3.5-180 | 2000 | 3.5 | 185.00 | 385.4 | 757.0 | 1078.1 | 2 | 28.4 | $\varphi$6.5@360 | 2$\varphi$8+2$\varphi$10 |
| BX-1-3.5-∞ | 2000 | 3.5 | 185.00 | 385.4 | 738.2 | 1125.9 | 1 | 27.5 | - | 2$\varphi$8+2$\varphi$10 |
| BX-2-3.5-∞ | 2000 | 3.5 | 185.00 | 385.4 | 757.0 | 1078.1 | 2 | 28.4 | - | 2$\varphi$8+2$\varphi$10 |

Table 3 Material properties of steel bars

| Steel category | Types | Yield strength (MPa) | Ultimate strength (MPa) | Elastic modulus (MPa) | Elongation (%) |
|---|---|---|---|---|---|
| Longitudinal reinforcement | φ10 | 485.64 | 593.25 | $1.92\times10^5$ | 10.67 |
| | φ8 | 514.53 | 646.84 | $1.88\times10^5$ | 17.00 |
| Stirrups | φ6.5 | 363.94 | 468.23 | $1.99\times10^5$ | 15.67 |

(in mm). The specimens with different key parameters are listed in Table 2.

### *2.2 Test setup and instrumentations*

All beams were loaded on an electro hydraulic servo-testing machine with a capacity of 500-kN. A four-point test procedure was followed where the specimens were subjected to sagging moment. Static load was applied by a traverse with constant speed of 0.2 kN/s underneath the beam using a hydraulic jack. When yield load was almost achieved, load was controlled by the deflection speed of the beam, which was 0.2±0.05 mm/s in this work. Several linear variable differential transformers (LVDT) were placed at the central point, loading point and midpoint between the loading point and support of the beams to measure displacements. Different load levels (first crack load, ultimate load, and failure load) were recorded and calculated and crack development was observed and marked. Then, a crack detection microscope (100×magnification with 0.01 mm least count) was used to precisely monitor crack widths development. Failure process, crack development and deflection of all tested beams were depicted as shown in Fig. 4.

## 3. Test result

### *3.1 Typical failure modes and corresponding load deformation curves*

Different failure modes and behaviors were observed based on the variation of longitudinal and transverse reinforcements, *S/D* ratios and steel fiber amounts. Fig. 4 shows failure processes and corresponding load deflection curves for tree different specimens.

In initial loading stage, all beams exhibited similar response, especially before the first crack was created. All beams showed linear behaviors and first cracks always appeared between two loading points. As loading was increased, other cracks were appeared in shear, flexure and bonding regions between steel shape flange and concrete, leading to failure.

Beams without steel fibers and conventional reinforcements showed relatively brittle failure modes at shear depth ratios of 2.5 and 3.5. The occurrence and development of bond cracks were the main reasons of failure, which resulted in the detachment of large pieces of concrete from the upper flange of steel shape, rapid degeneration of bearing capacity and serious spalling of concrete on the upper surfaces of beams (Fig. 4(a)). The number of cracks and beam deflections was obviously low. Thus, it was concluded that plastic deformation capabilities of beams were quite limited and decline segments after peak values were relatively quick.

Beams with steel fibers without longitudinal and transverse reinforcements exhibited relatively higher ductile bending failure rates at shear depth ratios of 2.5 and 3.5 (BY-2-2.5-∞ and BY-2-3.5-∞). When loading exceeded $0.8F_f$, the bottom flange of steel shape began to yield, load-deformation curve was close to horizontal line, deflection was significantly increased, bond cracks appeared in compressive zone (Fig. 4(a)) and a large number of branched cracks led to failure between two loading points. Finally, crushing of the concrete flange, dominated bending cracks extended to the upper flange of steel shape. By increasing steel fiber content to 2%, the number of bond cracks was significantly reduced and typical bond failure was transferred into bending failure significantly increasing

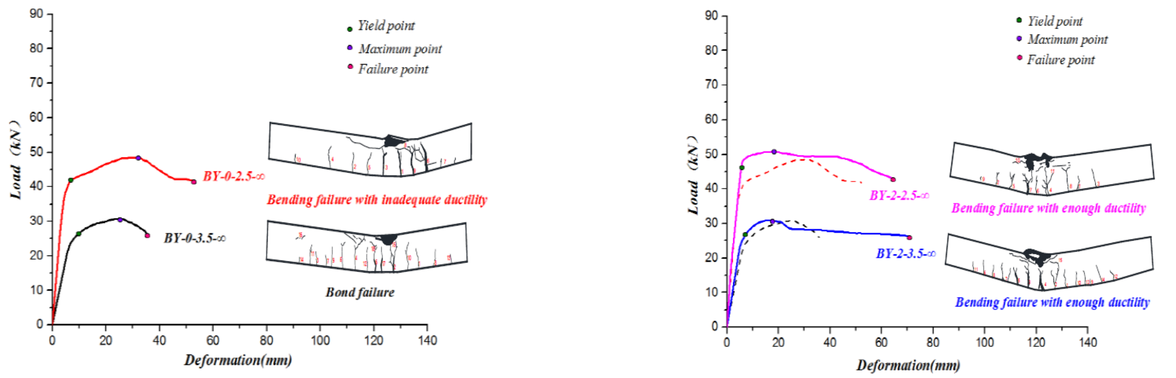


(a)Beams without steel bar

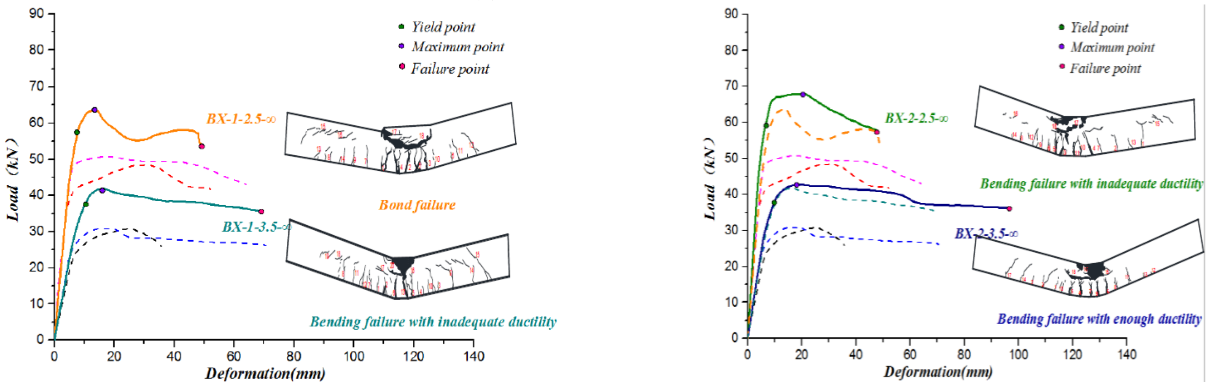


(b)Beams with longitudinal reinforcement

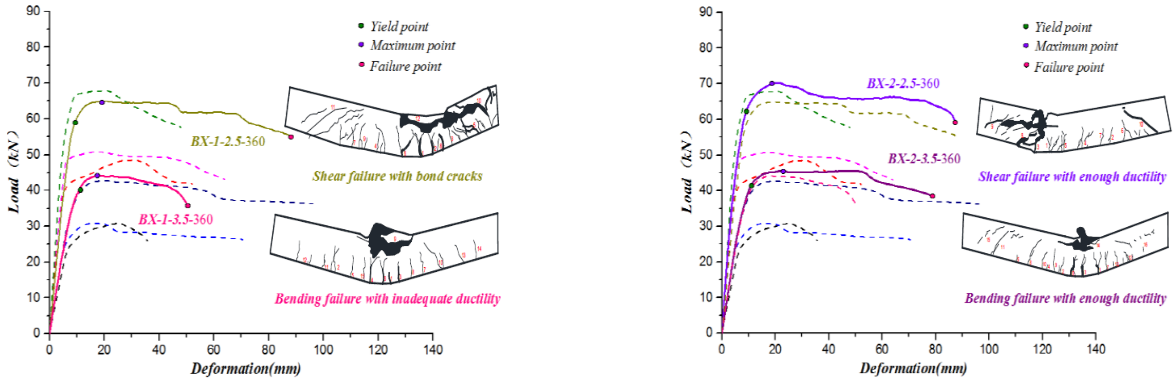


(c)Beams with longitudinal bar and stirrups

Fig. 4 Typical failure patterns and corresponding load-deflection curves

beam deflections. A long level or decline segments were observed after peak value in load-deflection curves.

Beams with steel fiber and longitudinal reinforcement showed bending and bonding combined failures. Severe bonding failure was observed for beams containing 1% steel fiber, a distinct arc bond crack dominated main failure mode, which appeared at about 80% of ultimate load. By increasing load, concrete was eventually peeled off the upper flange of steel shape. As for beams containing 2% steel fiber, specimens exhibited pure bending failures (Fig. 4(b)). Relatively rapid bending crack development and bond failures between steel shape flange and concrete interface appeared by increasing load, which resulted in great degeneration of the flexural rigidity of pure bending section and rapid increase of bending crack deflection and width. Concrete in middle-span compression zone was crushed under bending compressive stress and specimens were failed. The maximum bearing load was significantly increased with the addition of longitudinal reinforcement, but a sudden drop was observed after achieving maximum load value in curves, especially in BX-2-2.5-∞ beams. Therefore, plastic deformation capacity was found to be inadequate and this mode was expressed as “bending with inadequate or low ductility”. In contrast, load-deflection curve of BX-2-3.5-∞ had very good plumpness, with almost no significant decrease in segment.

The failure mode and damage pattern of this type of specimens (BX-1-3.5-360, BX-2-3.5-360, BX-1-3.5-180, BX-2-3.5-180, BX-1-2.5-180 and BX-2-2.5-180) were mainly bending and failure process was similar to the bending failure previously described for beams without stirrups. In addition, shear failure was observed in beams BX-1-2.5-360 and BX-1-2.5-360. Bond cracks were also appeared in beam BX-1-2.5-360 at 80% of maximum load.

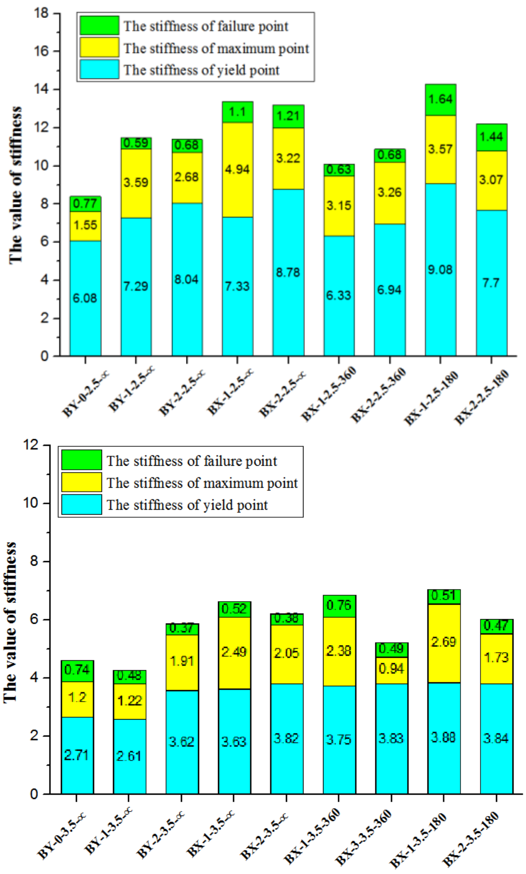


Fig. 5 Stiffness values of characteristic points

The two types of cracks were eventually connected and the specimen was failed. Stirrups encryption can restrict the development of shear and bond cracks to transform beam failure mode into flexural failure, but increasing the amount of steel fiber only eliminated bond cracks. The sudden through of the dominated diagonal shear crack and crushing and massive collapse of concrete at loading point were the main causes of the loss of bearing capacity in BX-2-2.5-360. The addition of stirrups also improved the ultimate load and ductility of specimens, but the magnitude of improvement was limited. Different from traditional brittle shear failure of reinforced concrete specimens, the descending portion of load deformation curve for beams BX-1-2.5-360 and BX-2-2.5-360 was flat and beams showed good ductility (Fig. 4(c)).

### *3.2 Stiffness of characteristic points and stiffness degradation curve*

The load, displacement and stiffness values of 3 characteristic points (yield, maximum and failure points) at loading point are listed in Table 4. Yield points (Park 1989), maximum points ($\Delta_y$) and failure load 0.85$F_m$ (Wu *et al.* 2018) are shown in Fig. 4. The stiffness of yield, maximum and failure points of bearing capacity ($K_y$, $K_m$ and $K_f$, respectively) of tested specimens were calculated from characteristic point loads divided by corresponding deflections, as shown in Fig. 5.

The addition of steel fiber and stirrups significantly improved the bearing capacity and stiffness of specimens. Therefore, crack resistance and suturing ability of steel fiber significantly improved bearing capacity stability. For short beams (*S/D*=2.5), when steel fiber content was increased from 0% to 1%, its strengthening effect was more pronounced and the rate of average stiffness improvements were nearly 20% and 132%, respectively, for yield and maximum stiffness. However, when steel fiber content was further increased to 2%, its strengthening effect on stiffness was more remarkable for long beams (*S/D*=3.5). This was because in long beams, bending cracks mainly dominated the failure mode, shear cracks rarely occurred, steel fiber content needed to be increased to a relatively high value (2%), and the improvement of steel fiber in flexural capacity was evident. Furthermore, when stirrup spacing was decreased to 180mm, the improvement effect of steel fiber was obviously weakened and the value of stiffness remained stable or even decreased.

Similar stiffness improvement was observed by shortening stirrup spacing since decreasing steel fiber content the stronger the enhancement of shortening stirrups spacing for stiffness. For beams containing 1% steel fiber, the average improvement of three characteristic stiffness values was close to 72% and 34% for short and long beams when stirrup spacing was decreased from 360mm to 180mm, but the corresponding improvement of stiffness was only 39% and 26% for short and long beams containing 2% steel fiber content, respectively.

Coefficient $\eta$ is defined as the ratio of stiffness $K$ of different displacement $\Delta$ divide by the initial stiffness $K_0$ and can be calculated as

$$\eta = \frac{K}{K_0} \tag{1}$$

which can reflect the degradation of stiffness. The initial elastic stiffness is adopted as $K_0$. Figs. 6 and 7 give the variation of $\eta$ during the whole loading process.

Based on the type of failure mode and above figures, the process of stiffness degradation was divided into three stages.

(1) The first stage was from the beginning to the yield of test, during which steel stayed in elastic condition. Although a large number of cracks were appeared, stitching of steel fibers for cracks made a considerable contribution to stabilizing stiffness value, which had only a small reduction mainly due to the presence of tiny cracks and nonlinear performance of concrete. Load deflection curves stayed almost linear during this period, while loading and unloading curves were almost superposed. Stiffness showed good stability in this stage.

(2) The second stage comprised from yield to maximum response. The appearance of shear and bend cracks and development of crack width at this stage led to the acceleration of stiffness degradation and therefore the enhancement of steel fiber became decelerated. Especially, due to bond crack developments, interactions between both materials became weaker which also led to stiffness degradation.

(3) The third stage comprised from ultimate condition to failure condition. Few new cracks appeared during this stage, so stiffness degradation was slowed down. However,

Table 4 Summary of twenty one SFSRC specimens

| Specimen | Load(kN) | | | Displacement(mm) | | | Stiffness (kN· mm$^{-1}$) | | |
|---|---|---|---|---|---|---|---|---|---|
| | $F_y$ | $F_m$ | $F_f$ | $\Delta_y$ | $\Delta_m$ | $\Delta_f$ | $K_y$ | $K_m$ | $K_f$ |
| BY-0-2.5-∞ | 41.46 | 48.45 | 41.18 | 6.99 | 31.20 | 53.60 | 6.08 | 1.55 | 0.77 |
| BY-1-2.5-∞ | 43.52 | 50.20 | 42.67 | 5.98 | 14.00 | 71.75 | 7.29 | 3.59 | 0.59 |
| BY-2-2.5-∞ | 47.67 | 50.80 | 43.18 | 5.93 | 18.95 | 63.73 | 8.04 | 2.68 | 0.68 |
| BX-1-2.5-∞ | 57.50 | 63.60 | 54.06 | 7.85 | 12.87 | 49.18 | 7.33 | 4.94 | 1.10 |
| BX-2-2.5-∞ | 59.82 | 67.90 | 57.72 | 6.82 | 21.08 | 47.85 | 8.78 | 3.22 | 1.21 |
| BX-1-2.5-360 | 58.95 | 64.95 | 55.21 | 9.31 | 20.64 | 88.12 | 6.33 | 3.15 | 0.63 |
| BX-2-2.5-360 | 61.57 | 70.20 | 59.67 | 8.87 | 21.55 | 87.28 | 6.94 | 3.26 | 0.68 |
| BX-1-2.5-180 | 61.37 | 70.40 | 59.84 | 6.77 | 19.70 | 36.44 | 9.08 | 3.57 | 1.64 |
| BX-2-2.5-180 | 64.46 | 74.40 | 63.24 | 8.38 | 24.20 | 43.88 | 7.70 | 3.07 | 1.44 |
| BY-0-3.5-∞ | 26.41 | 30.80 | 26.18 | 9.80 | 25.73 | 35.50 | 2.71 | 1.20 | 0.74 |
| BY-1-3.5-∞ | 26.20 | 30.20 | 25.67 | 10.05 | 24.75 | 53.02 | 2.61 | 1.22 | 0.48 |
| BY-2-3.5-∞ | 26.99 | 30.90 | 26.27 | 7.48 | 16.15 | 70.57 | 3.62 | 1.91 | 0.37 |
| BX-1-3.5-∞ | 37.96 | 41.80 | 35.53 | 10.47 | 16.82 | 68.80 | 3.63 | 2.49 | 0.52 |
| BX-2-3.5-∞ | 38.20 | 42.70 | 36.30 | 10.01 | 20.80 | 96.30 | 3.82 | 2.05 | 0.38 |
| BX-1-3.5-360 | 39.84 | 44.10 | 37.49 | 10.64 | 18.55 | 49.08 | 3.75 | 2.38 | 0.76 |
| BX-2-3.5-360 | 41.19 | 45.55 | 38.72 | 10.77 | 48.64 | 78.49 | 3.83 | 0.94 | 0.49 |
| BX-1-3.5-180 | 42.22 | 45.95 | 39.06 | 10.90 | 17.10 | 76.95 | 3.88 | 2.69 | 0.51 |
| BX-2-3.5-180 | 42.27 | 46.90 | 39.87 | 11.03 | 27.10 | 85.17 | 3.84 | 1.73 | 0.47 |

cracks were extended and slippage occurred at the interface of concrete and steel with the development of bond cracks. Shear cracks penetrated the whole section and bending cracks tended to develop to the top flange of steel shape. Hence, load deflection curves showed obvious decrease at this stage, which became much more serious if the volume content of stirrups and steel fibers were small.

The influence of steel fiber on the curve was evident. The addition of steel fiber apparently slowed down the slope of curve, especially for specimens without conventional reinforcement. The value of $\eta$ at failure points of specimens BY-1-2.5-∞ and BY-2-3.5-∞ were 0.05 and 0.06 with deflections of 71.7 mm and 70.5 mm, respectively. However, corresponding values for BY-0-2.5-∞ and BY-0-3.5-∞ beams were 0.07 and 0.13 with deflection of 53.6mm and 35.5 mm, respectively (Fig. 6(a)). It is noteworthy that beams with 1% steel fiber showed excellent degradation of stiffness curves, but increasing steel fiber content to 2% did not further improve their performance as stiffness degradation was unexpectedly accelerated. For beams with steel bars, the factors affecting curve trend were very complicated. The variation patterns of stiffness curves were sensitive to the percentages of steel fiber and stirrup spacing and the effect of steel fiber was obviously weakened with the addition of stirrups (Fig. 6 (b)-(c)). Stirrup spacing dominated the variation of the value of $\eta$, especially for short beams. The value of $\eta$ at the failure point of specimen BX-1-2.5-∞ was 0.10 with deflection of 49.1 mm. Addition of stirrups with spacing of 360 mm decreased the corresponding value to 0.07 with deflection of 88.1 mm (Fig. 7). The descending part of the curve was most gentle for beams with stirrup spacing of 360 mm. However, these variable parameters seemed to have little effects on long beams with most curves almost coinciding. This was because bending cracks were the main reason of failure in long beams. The addition of steel fiber and stirrups had relatively little effect on this type of beams.

### 3.4 Damage analysis

In the bending tests of SFSRC beams, the essence of failure was damage development and accumulation in specimens. In order to quantitatively describe bending damage process in SFSRC beams, the concept of damage degree (Roufaiel and Meyer 1987) was adopted and the variation of secant stiffness of load-deflection curves was quantitatively analyzed. At initial loading stage, when specimens were in uncracking stage, damage degree was $D$=0. By increasing load, the damage of specimens began to accumulate and develop gradually increasing damage degree. When the bearing capacity of specimens was decreased to 85% of the maximum load $F_m$ due to the accumulation of damage, specimens were considered as failed and damage degree was increased to 1.0. The expression was stated as

$$D = \frac{K_{\mathrm{r}}\left(K_0 - K_{\mathrm{i}}\right)}{K_{\mathrm{i}}\left(K_0 - K_{\mathrm{r}}\right)} \tag{2}$$

In the above equation, $K_0$ is the initial elastic stiffness of load-displacement curve, $K_i$ is the secant stiffness of any point to the original point in load-displacement curve, i.e., stiffness at any loading time, and $K_r$ is the secant stiffness of failure point to the original point of load-displacement curve calculated as $K_r$=$F_f$/$\Delta_r$. The detailed calculated method is shown in Fig. 8(a).

As shown in Fig. 8(b)-(d), the damage development of specimens with steel fibers were obviously slower than those without steel fibers. The application of steel fiber in specimens effectively delayed damage accumulation. Moreover, increasing the content of steel fiber also delayed damage development in specimens and lower amounts of

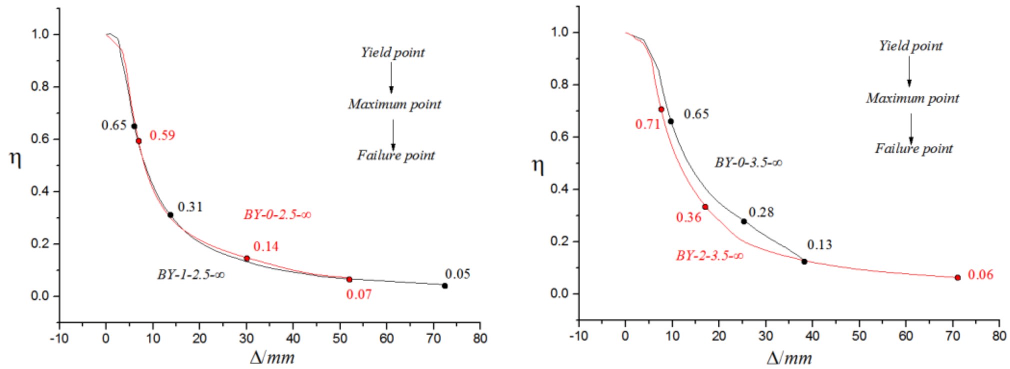


(a) Beams without steel bar

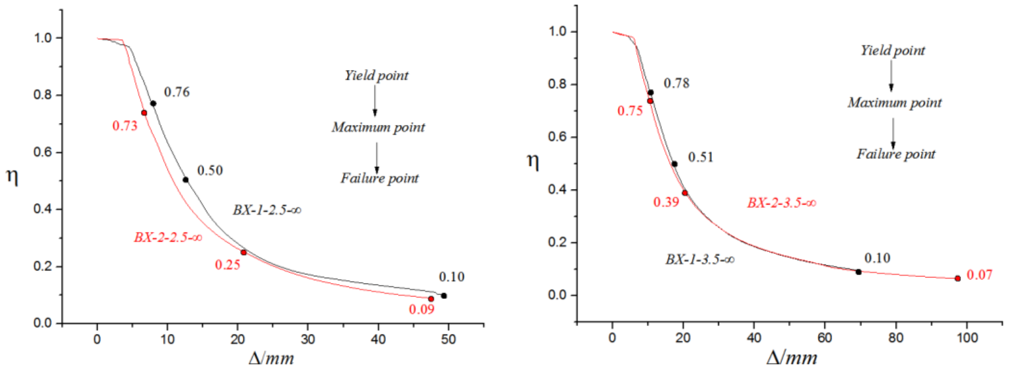


(b) Beams with longitudinal bar

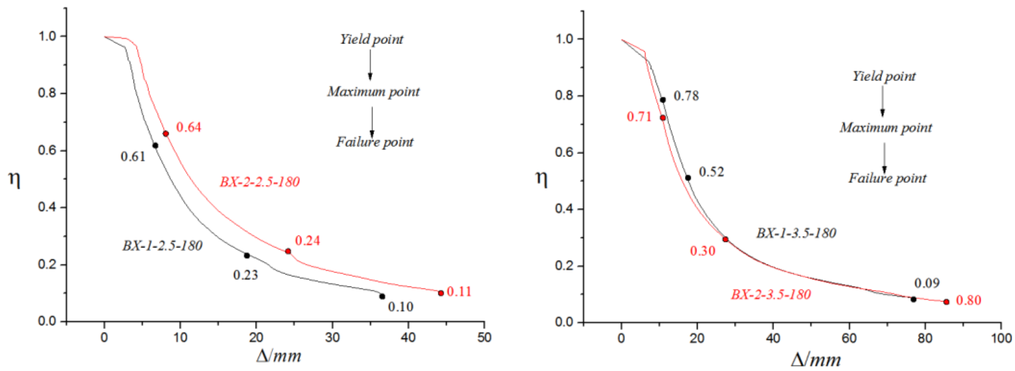


(c) Beams with steel reinforced cage

Fig. 6 Influence of steel fiber for stiffness degradation curve

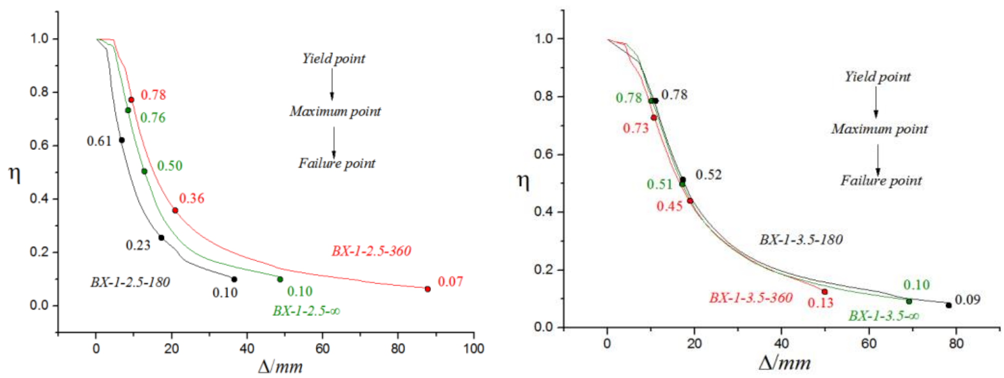


Fig. 7 Influence of stirrup for stiffness degradation curve

steel fiber resulted in faster damage development. In the case of high amounts of steel fiber, bond strength between steel and concrete was greatly improved because of the effective control of steel fiber on bond cracks and the bond failure of the specimens was effectively decreased. At the same time, the development of shear and bending cracks in

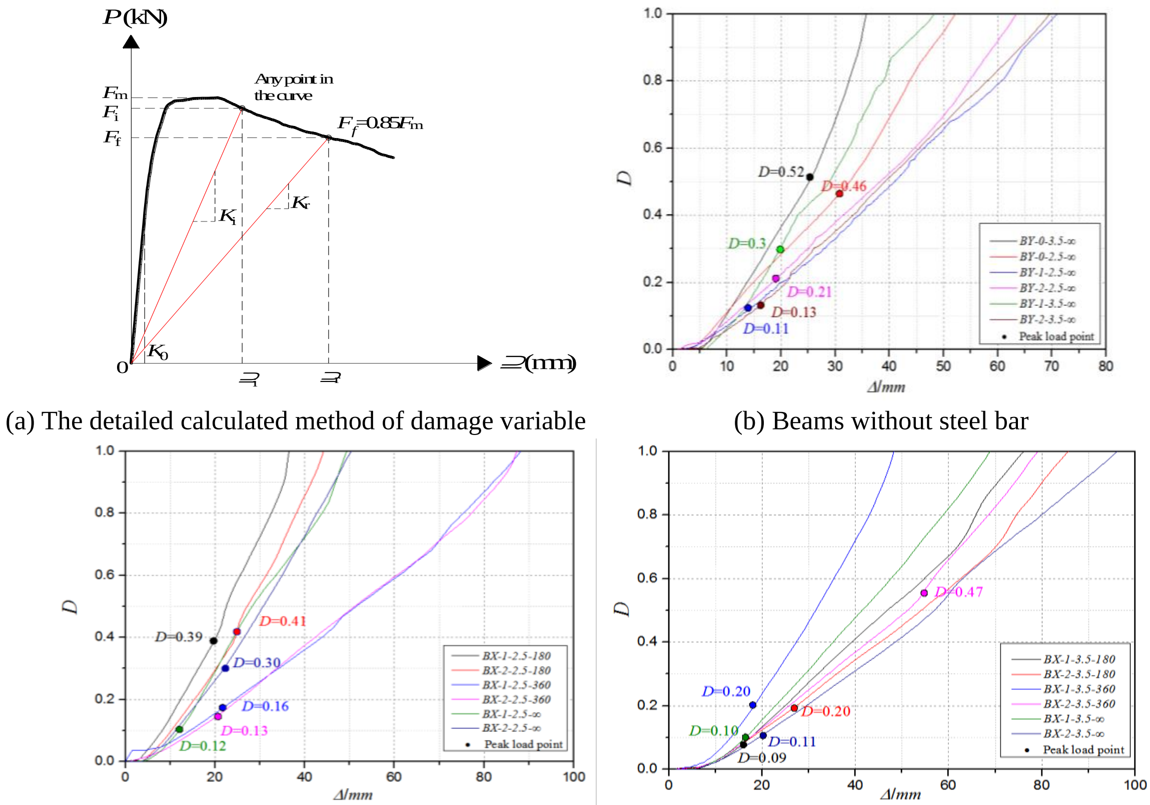


(a) The detailed calculated method of damage variable (b) Beams without steel bar

(c) Beams with steel bar

Fig. 8 The calculation and growth development of damage

concrete specimens was also restrained and damage accumulation was decelerated making the specimen more stable.

For short beams ($S/D$=2.5) with steel bars, stirrups had a significant effect on damage development rate. At stirrup spacing of 180mm, damage development with the increase of deflection was faster than that in specimens without reinforcement; damage development rate in specimens with stirrup spacing of 360mm was the lowest. When deflection was increased to 40mm, damage degree of specimen BX-1-2.5-180 had already reached 1.0. At the same time, the damage degrees of BX-1-2.5-0 and BX-1-2.5-360 were 0.72 and 0.33, respectively. Damage development rate did not decrease with monotonous increase of stirrup volume due to relatively complex failure modes of short beams. The enhancement of steel fibers and stirrups was affected by the variation of failure mode. Different damage development trends were observed for long beams ($S/D$=3.5) with steel bars. The dominant failure mode of long beams was ductile bending failure and increasing the amount of stirrups significantly restrained damage development. When deflection reached around 77mm, specimen BX-1-3.5-180 was failed. However, the failure deflections of BX-1-3.5-∞ and BX-1-3.5-360 specimens were 68.8mm and 49.1mm, respectively. Adding more stirrups obviously restrained damage development. Damage development in specimens with higher steel fiber contents was relatively slower. The 12 specimens in Fig. 8(c) showed the same law, which was consistent with the law of the specimens without steel bars.

For specimens BY-0-2.5-∞ and BY-0-3.5-∞, the damage degree of maximum load $D_m$ was equal to 0.46 and 0.52, respectively. While Steel fibers had a remarkable effect in controlling crack development (especially bonded cracks) and restraining damage development before peak load, the damage degree at peak load was greatly reduced, such that the damage degree of maximum loads $D_m$ for specimens BY-1-2.5-∞ and BY-1-3.5-∞ were decreased to 0.11 and 0.3 and $D_m$ for specimens BY-2-2.5-∞ and BY-2-3.5-∞ reached only 0.21 and 0.13, respectively. The above results showed increasing the amount of steel fibers improved the damage resistance of specimens at peak load and ultimate bearing capacity was maintained even under severe damage conditions.

Different trends were observed for 12 beams with steel bars. When steel fiber content was increased from 1% to 2%, specimen damage under peak load was aggravated. The influence of steel fiber content on peak load damage was determined by stirrups and shear span ratio, while the enhancement of steel fibers in the damage resistance of specimens under peak load was alleviated with the addition of stirrups. For beams BX-1-2.5-∞, BX-2-2.5-∞, BX-1-3.5-∞ and BX-2-3.5-∞ without stirrups, when steel fiber content was increased from 1% to 2%, $D_m$ was increased from 0.12 to 0.30 for short beams and from 0.10 to 0.11 for long beams. Adding stirrups into specimens also had a significant effect on peak load damage. For short beams, the value of peak load damage simply rose from 0.39 to 0.41 and 0.13 to 0.16, respectively. For beams with stirrup spacing of 180 mm and 360 mm, when steel fiber content was increased from 1% to 2%, the value of peak load

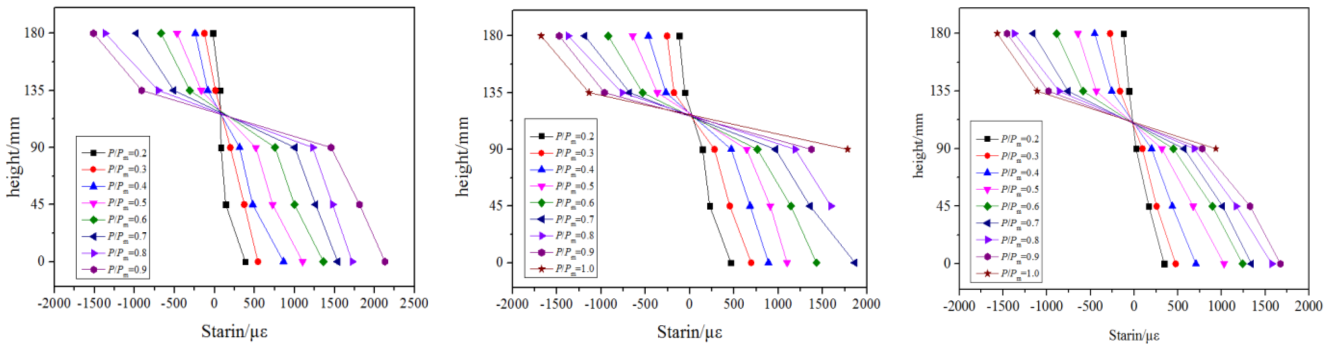


(a) BY-1-3.5-∞ (b) BX-2-3.5-360 (c) BX-1-3.5-180

Fig. 9 Strain distribution curves along the section height

damage remained almost unchanged. However, increasing shear span ratio enhanced the effect of steel fiber on peak load damage. The value of peak load damage was increased from 0.09 to 0.20 and 0.21 to 0.47 for beams with stirrups spacing of 180 mm and 360 mm, respectively, and when steel fiber content was increased from 1% to 2%, the magnitude of improvement tended to be 122% and 124%, respectively.

In general, for specimens without stirrups, only steel fibers restrained the occurrence and development of bond and shear cracks while improving concrete brittleness. Therefore, the damage resistance of specimens at peak load was greatly affected by the addition of steel fibers. For specimens with stirrups, stirrups and steel fibers worked together to improve the damage resistance of specimens in which stirrups played a dominate role; thus the influence of steel fibers was greatly weakened.

### *3.5 Validation of the plane section assumption*

The strain variation along the height of concrete section can reflect the interaction of steel shape and concrete to a certain extent. As a conventional procedure, five strain gauges was arranged along the entire height of the section to verify the section assumption. Fig. 9 shows the strain distribution of the concrete during the whole loading process in the beams BY-1-3.5-∞, BX-2-3.5-360 and BX-1-3.5-180, and the result agrees with the theory, in which strain is almost linearly distributed along the height of the concrete throughout the loading process.

## 4. Predicted formulas of bending stiffness

For calculating the bending stiffness of SFSRC specimens before yielding, the following conditions were assumed:

1. Plane section assumption was fulfilled.
2. The tensile stress of SFRC considered.
3. Due to the restraint of steel shape, concrete core zone did not crack at service stage.

For SFSRC beams without steel bars, bending stiffness $B$ was calculated by the summation of stiffness of steel shape and outer SFRC. Due to the addition of steel fibers, the tensile area of cracked concrete still bore a fraction of

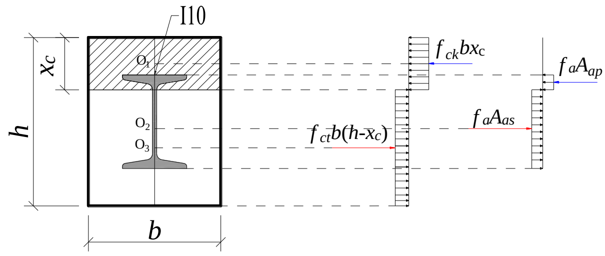


Fig. 10 Stress distribution of cross section for beams without steel bar

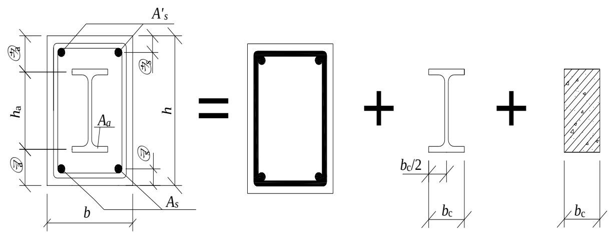


Fig. 11 Computing pattern of bending stiffness

tensile force. Therefore, in this paper, based on geometrical relationship in section before cracking, stiffness reduction coefficient $\alpha_z$ was introduced to consider the effect of steel fiber on stiffness after cracking and bending stiffness equations were presented.

$x_c$ is the height of compressive zone and was calculated based on stress distribution of cross section shown in Fig. 11 as

$$x_c = \frac{f_{ct}bh + (A_{as} - A_{ap}) f_a}{f_{ck}b + f_{ct}b} \tag{3}$$

where $A_{as}$ and $A_{ap}$ are the tensile and compression areas of steel shape and $f_{ck}$ is the axial compressive strength of concrete given by $f_{ck}$=0.67 $f_{cm}$ (50010-2010 2010). The tensile stress of SFRC $f_{ct}$ can be calculated as $f_{ct} = f_t(1+a_t\lambda_f)\beta_{tu}\lambda_f$ (38-2004 2004). The characteristic value of steel fiber $\lambda_f$ was calculated as $\lambda_f = \rho_f \cdot l_f / d_f$ (38-2004, 2004). In order to simplify calculations, bending stiffness of beams without steel bars were calculated as

$$B = \alpha_z\{E_{fc}[\frac{1}{12}bh^3 + bh(\frac{h}{2} - x_c)^2] + E_a[I_a + A_a(\frac{h}{2} - x_c)^2]\} \tag{4}$$

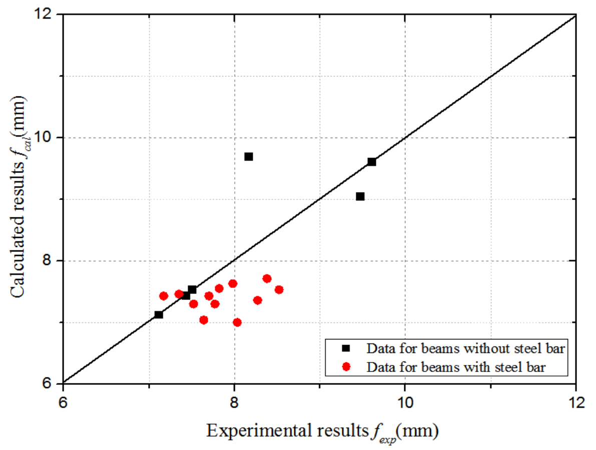


Fig. 12 Comparisons between experiments and predictions of the proposed formula

A reduction coefficient $\alpha_z$ was used to consider the influence of bond slip between steel shape and concrete, which was calculated based on test results (Table 5) as

$$\alpha_z = 0.18(1+0.06\lambda_f) \tag{5}$$

Based on a previous research (Zheng and Li 2012), the bending stiffness $B$ of SFSRC beams with steel bars under the condition of short term load was calculated by Eq. (6) based on computing pattern illustrated in Fig. 12.

$$B = B_{sf} + B_a + B_c \tag{6}$$

where $B_{sf}$ is the stiffness of steel fiber reinforced concrete and was calculated by Eq. (7) based on CECS 38:2004 (38-2004, 2004), $B_a$ is the stiffness of steel shape and $B_c$ is the stiffness of concrete rigid core area.

$$B_{sf} = B_{rc}(1+\lambda_f \beta_B) \tag{7}$$

The stiffness of reinforcement concrete $B_{rc}$ was calculated by Eq. (8) (GB50010-2010, 2010) as

$$B_{rc} = \frac{E_S A_s h_0^2}{1.15\varphi + 0.2 + \dfrac{6\alpha_E \rho}{1+3.5\gamma_f'}} \tag{8}$$

where $\gamma_f'$ is the ratio of effective area of tension flange to web, $\beta_B$ is the influence of steel fiber on short term stiffness of beams and equal to 0.11(Gao and Zhang 2013), $\varphi$ is the nonuniformity coefficient of longitudinal tensile reinforcement between two cracks. $h_0$ is the effective height of section, $h_0 = h - a_s$; $\alpha_E = E_S/E_{fc}$; $\rho = A_S/(b-b_c)h_0$; $\gamma_f' = b_c a_s'/(b-b_c)h_0$ . $\rho$ is reinforcement ratio of longitudinal tension steel bar. It was assumed that concrete core zone did not crack at service stage.

$B_a$ was calculated as

$$B_a = E_a[I_a + A_a(\frac{h_a}{2} + a_s' - \bar{x})^2] \tag{9}$$

where $I_a$ is the moment of steel inertia and $A_a$ is steel shape section area. The stiffness of rigid core area was calculated as

Table 5 The characteristics of specimens and comparisons between the experiments and predictions

| Specimen | $F$ (kN) | $f_{exp}$ (mm) | $f_{cal}$ (mm) | $f_{cal}/f_{exp}$ (mm) | Specimen | $F$ (kN) | $f_{exp}$ (mm) | $f_{cal}$ (mm) | $f_{cal}/f_{exp}$ (mm) |
|---|---|---|---|---|---|---|---|---|---|
| BY-0-2.5-∞ | 41.40 | 7.43 | 7.44 | 1.00 | BY-0-3.5-∞ | 25.25 | 9.60 | 9.61 | 1.02 |
| BY-1-2.5-∞ | 43.61 | 7.50 | 7.61 | 1.04 | BY-1-3.5-∞ | 24.45 | 9.47 | 9.05 | 1.01 |
| BY-2-2.5-∞ | 41.85 | 7.11 | 7.13 | 1.18 | BY-2-3.5-∞ | 26.90 | 8.16 | 9.70 | 0.87 |
| BX-1-2.5-∞ | 54.09 | 8.03 | 7.00 | 0.93 | BX-1-3.5-∞ | 32.27 | 7.82 | 7.55 | 1.25 |
| BX-2-2.5-∞ | 57.76 | 7.17 | 7.43 | 1.06 | BX-2-3.5-∞ | 31.70 | 8.27 | 7.36 | 0.96 |
| BX-1-2.5-360 | 54.40 | 7.64 | 7.04 | 0.78 | BX-1-3.5-360 | 32.96 | 8.38 | 7.71 | 1.00 |
| BX-2-2.5-360 | 57.77 | 7.7 | 7.43 | 1.06 | BX-2-3.5-360 | 31.43 | 7.77 | 7.30 | 1.08 |
| BX-1-2.5-180 | 56.35 | 7.52 | 7.30 | 1.09 | BX-1-3.5-180 | 32.20 | 8.52 | 7.53 | 1.08 |
| BX-2-2.5-180 | 58.00 | 7.35 | 7.46 | 1.13 | BX-2-3.5-180 | 32.85 | 7.98 | 7.63 | 1.08 |
| Mean | | | | | | 0.97 | | | |
| Standard deviation | | | | | | 0.07 | | | |
| Coefficient of variation | | | | | | 0.07 | | | |

$$B_c = E_{fc}[\frac{1}{12}b_c h_a^3 + b_c h_a(\frac{h_a}{2} + \alpha_s' - \bar{x})^2] \tag{10}$$

where $E_{fc}$ is elastic modulus of steel fiber concrete and $\bar{x}$ is the average height of neutral axis and was calculated based on Zheng's theory (Zheng and Li 2012)

$$\bar{x} = \int_0^{l_{cr}} sdz / l_{cr} = 0.5(x_c + x_{\max}) \tag{11}$$

$x_{\max}$=0.5$h$ and the depth of compressive zone for cracked section was calculated as

$$\alpha_E(A_s + A_s' + A_a)(d - x_c) = \frac{1}{2}bx_c^2 \tag{12}$$

where

$$d = \frac{[a_s' A_s' + (h - a_s - \frac{h_a}{2})A_a + (h - a_s)A_s]}{[A_s + A_s' + A_a]} \tag{13}$$

In order to verify the accuracy of bending stiffness equations, the calculated values were used to define mid span deflection $f$ using structural mechanics method. The experimentally obtained results are listed in Table 5 which indicated that the calculated results were almost equal to tested deflections. Therefore, stiffness equations presented in this paper objectively reflected the in-plane bending deformation resistance of beam members under short-term loads and were suitable for deflection calculation of SFSRC beams.

$$f = \frac{Fa}{24B}(3l^2 - 4a^2) \tag{14}$$

where: *F* is the load of the loading point, *a* is the distance of the shear span and *l* is the length of the tested beam.

The bending stiffness calculated from proposed predicted formulas are compared with the experimental results shown in Table 5 and Fig. 13, and good agreement is achieved between them. The mean value of $f_{exp}/f_{cal}$ ratio is 0.97 with the corresponding coefficient of variation (*COV*) of 0.07. It can be indicated that this calculation model is feasible for predicting the bending stiffness of steel fiber steel reinforcement concrete specimens under bending within acceptable limits.

## 5. Conclusions

In this paper, experimental results of four-point bending test on 18 SFSRC beams reinforced with conventional reinforcements and steel fibers were presented. The failure modes, stiffness degradation and damage development of SFSRC specimens were also investigated. Based on the above analysis, following conclusions were drawn:

1. Just like stirrups, steel fibers played an important role in the failure modes of SFSRC specimens, especially in restricting bond and shear cracks. With the increase of steel fiber content, shear and bond cracks were significantly decreased.
2. The addition of steel fibers seemed to have a minor effect on the bearing capacity of SFSRC beams. Maximum bearing load improvement was relatively small, especially for bending strength. However, the stability of bearing capacity was apparently enhanced. Increasing steel fibers content, stabilized the falling section of load-deflection curve.
3. Stiffness of characteristic points and stiffness degradation curve during the whole loading process were evaluated and it was found that the addition of steel fiber and stirrups significantly improved the bearing capacity and stiffness of specimens. With the addition of stirrups and increase of shear span depth ratio, the variation of stiffness became complicated and enhancement of steel fiber for stiffness was obviously weakened.
4. By increasing steel fiber content, the damage degree of the peak load of specimens was seriously increased. By increasing the content of steel fiber, damage resistance of specimens under peak load was improved and their ultimate bearing capacity was maintained even under severe damage conditions. The damage resistance of specimens under peak load was greatly affected by steel fiber content. For beams with conventional reinforcements, both stirrups and steel fibers enhanced the damage resistance of specimens where stirrups plays essential much more important role, thus the influence of steel fiber was greatly weakened.
5. Equations were derived to calculate the bending stiffness of SFSRC specimens which were used to define the deflection of the mid-span of beams. The accuracy of the calculation method was proven by comparing predicted and experimental results.

## Acknowledgement

This work is supported by National Natural Science Foundation of China (Grant No.51208175), Natural Science Foundation of Anhui Provincial Department of Education (Grant No.KJ2018A0478), the Fundamental Research Funds for the Central Universities (Grant No.2015B17514;2016B20514) and National innovation and entrepreneurship training program for College Students (Grant No. 201910383110)

## Reference

ACI318-11 (2011), 318, Building Code Requirements for Structural Concrete (ACI318-11) and Commentary, ACI318-11, American Concrete Institute, Farmington Hills, MI, USA.

Anderson, D. (2014), Eurocode 4-Design of Composite Steel and Concrete Structures.

Aoude, H., Belghiti, M., Cook, W.D. and Mitchell, D. (2012), "Response of steel fiber-reinforced concrete beams with and without stirrups", *ACI Struct. J.*, **109**(3), 359-367.

Biolzi, L. and Cattaneo, S. (2017), "Response of steel fiber reinforced high strength concrete beams: Experiments and code predictions", *Cement Concrete Compos.*, **77**, 1-13.

Biolzi, L., Cattaneo, S. and Guerrini, G.L. (2000), "Fracture of plain and fiber-reinforced high strength mortar slabs with EA and ESPI monitoring", *Appl. Compos. Mater.*, **7**(1), 1-12.

CECS 38-2004 (2004), Technical Specifications for Fiber Reinforced Concrete Structures, China Plan Press, Beijing, China.

CECS38:92 (1992), Specification for Design and Construction of Steel Fiber Reinforcement Concrete Structures, China Association for Engineering Construction Standardization, Beijing, China.

Chen, Z., Chen, Y., Zheng, H. and Xue, J. (2013), "Analysis of influence factors and bond strength of steel-recycled aggregate concrete interface", *Indus. Constr.*, **43**(9), 1-6.

Chen, Z., Zhou, W. and Xu, J. (2015), "Experimental study on bond-slip behavior of steel reinforced high strength concrete after high temperature", *J. Build. Struct.*, **36**(12), 106-115.

Chen, Z.P., Liang, Y. and Chen, Y.L. (2014), "Research on bonding strength of steel and concrete with different bonding interfaces", *Appl. Mech. Mater.*, **470**, 838-841.

Ding, Y., Zhang, F., Torgal, F. and Zhang, Y. (2012), "Shear behaviour of steel fibre reinforced self-consolidating concrete beams based on the modified compression field theory", *Compos. Struct.*, **94**(8), 2440-2449.

Dinh, H.H., Parra-Montesinos, G.J. and Wight, J.K. (2010), "Shear strength model for steel fiber reinforced concrete beams without stirrup reinforcement", *J. Struct. Eng.*, **137**(10), 1039-1051.

Eltobgy, H.H. (2013), "Structural design of steel fibre reinforced concrete in-filled steel circular columns", *Steel Compos. Struct.*, **14**(3), 267-282.

Fantilli, A.P., Vallini, P. and Chiaia, B. (2011), "Ductility of fiber-reinforced self-consolidating concrete under multi-axial compression", *Cement Concrete Compos.*, **33**(4), 520-527.

FIB. (2013), fib Model Code for Concrete Structures 2010, 978-3-433-03061-5, Ernst Sohn Pub.

Foraboschi, P. (2016), "Versatility of steel in correcting construction deficiencies and in seismic retrofitting of RC buildings", *J. Build. Eng.*, **8**, 107-122.

Gao, D.Y. and Zhang, M. (2013), "Calculation method for stiffness of steel fiber reinforced high-strength concrete beams based on effective moment of inertia", *China J. Highw. Tran.*, **26**(5), 62-68.

GB 50010-2010 (2010), Code for Design of Concrete Structures, China Building Industry Press, Beijing, China.

Jang, S.J. and Yun, H.D. (2018), "Combined effects of steel fiber and coarse aggregate size on the compressive and flexural toughness of high-strength concrete", *Compos. Struct.*, **185**, 203-211.

JG-T 472-2015 (2015), Steel Fiber Reinforced Concrete, Ministry of Housing and Urban Rural Development of People's Republic of China, Beijing, China.

JGJ138-2016 (2016), Code for Design of Composite Structures, Ministry of Housing and Urban Rural Development of People's Republic of China, Beijing, China.

Kim, K.S., Lee, D.H., Hwang, J.H. and Kuchma, D.A. (2012), "Shear behavior model for steel fiber-reinforced concrete members without transverse reinforcements", *Compos. Part B: Eng.*, **43**(5), 2324-2334.

Li, J., Qiu, D. and Yu, K. (2015), "Study on bond-slip behavior between spaped steel and concrete in SRC structures after exposed to high temperature", *En. Mech.*, **32**(2), 190-200.

Li, J., Wang, G., Qiu, D. and Yu, K. (2012), "Study on the force transfer behavior of SRC members with stud shear connectors", *China Civil Eng. J.*, **45**(12), 74-82.

Park, R. (1989), "Evaluation of ductility of structures and structural assemblages from laboratory testing", *Bull. NZ Nat. Soc. Earthq. Eng.*, **22**(3), 155-166.

Roufaiel, M.S. and Meyer, C. (1987), "Analytical modeling of hysteretic behavior of R/C frames", *J. Struct. Eng.*, **113**(3), 429-444.

Shansuo, Z., Guozhuan, D., Yong, Y., Maohong, Y. and Junfeng, Z. (2003), "Experimental study on bond-slip performance between steel shape and concrete in SRC structures", *Eng. Mech.*, **20**(5), 63-69. (in Chinese)

Tao, Z. and Yu, Q. (2012), "Residual bond strength in steel reinforced concrete columns after fire exposure", *Fire Saf. J.*, **53**, 19-27.

Wang, W.H., Han, L.H., Tan, Q.H. and Tao, Z. (2017), "Tests on the steel-concrete bond strength in steel reinforced concrete (SRC) columns after fire exposure", *Fire Technol.*, **53**(2), 917-945.

Won, J.P., Hong, B.T., Choi, T.J., Lee, S.J. and Kang, J.W. (2012), "Flexural behaviour of amorphous micro-steel fibre-reinforced cement composites", *Compos. Struct.*, **94**(4), 1443-1449.

Wu, K., Chen, F., Chen, C., Zheng, H. and Xu, J. (2019), "Analysis of the load transfer mechanism and bond stress components in Steel and Steel Fiber Reinforced Concrete (SSFRC) structure", *J. Struct. Eng.*, ASCE, **145**(12), 04019160.

Wu, K., Chen, F., Xu, F., Xu, J. and Xu, C. (2019), "Experimental study on interfacial bonding property and energy dissipation capacity between shape steel and steel fiber reinforced concrete", *China Civil Eng. J.*, 3.

Wu, K., Xue, J., Nan, Y. and Zhao, H. (2018), "Analysis on extension length of shape steel in transfer columns of SRC-RC hybrid structures", *Int. J. Steel Struct.*, **18**(3), 910-923.

Xu, C., Fukada, S. and Masuya, H. (2016), "The impact vibration-based fatigue damage assessment of steel and steel fiber reinforced concrete composite girder", *Int. J. Steel Struct.*, **16**(4), 1217-1226.

Xu, C., Su, Q. and Masuya, H. (2017), "Static and fatigue performance of stud shear connector in steel fiber reinforced concrete", *Steel Compos. Struct.*, **24**(4), 467-479.

Yang, Y. (2003), "Study on the basic theory and its application of bond-slip between steel shape and concrete in SRC structures", Ph.D. Dissertation, Xi'an University of Architecture and Technology, Xi'an, China.

YB9082-2006 (2006). Technical Specification for Steel Reinforced Concrete Structures, Metallurgical Industry Press, Beijing, China.

Ying, W. and Chen, Z. (2016), "Interface bond force transfer mechanisms and its influence analysis between shape steel and high-strength concrete", *China Civil Eng. J.*, **49**(9), 53-63.

Yoo, D.Y., Shin, H.O., Yang, J.M. and Yoon, Y.S. (2014), "Material and bond properties of ultra high performance fiber reinforced concrete with micro steel fibers", *Compos. Part B: Eng.*, **58**, 122-133.

Zheng, H., Chen, Z. and Su, Y. (2016), "Research on mechanical behavior and bearing capacity calculation method of steel reinforced recycle aggregate concrete combined component with stud connecters", *Indus. Constr.*, **46**(11), 97-104.

Zheng, H., Chen, Z. and Xu, J. (2016), "Bond behavior of H-shaped steel embedded in recycled aggregate concrete under push-out loads", *Int. J. Steel Struct.*, **16**(2), 347-360.

Zheng, S.S. and Li, l. (2012), *Basic Performance and Design of Steel Reinforced High Strength and High Performance Concrete Structure*, The Science Publishing Company, Beijing, China.

*CC*